
# Enhancement of Heat Transfer of Mixing Convection in a Vertical Channel by a Moving Block


W.-S. Fu, J.-C. Huang, Y.-Y. Wang and Y. Huang



Journal of Mechanics / Volume 29 / Issue 01 / March 2013, pp 95 - 107
DOI: 10.1017/jmech.2012.111, Published online: 08 February 2013

# ENHANCEMENT OF HEAT TRANSFER OF MIXING CONVECTION IN A VERTICAL CHANNEL BY A MOVING BLOCK

**W.-S. Fu** * **J.-C. Huang** **Y.-Y. Wang** **Y. Huang**

*Department of Mechanical Engineering*
*National Chiao Tung University*
*Hsinchu, Taiwan 30010, R.O.C.*

**ABSTRACT**

Enhancement of a heat transfer rate of mixed convection flow in a three-dimensional vertical channel with insertion of a moving slender block is investigated numerically. A slender block is installed along the direction of the channel flow, and the movement of the slender block is in periodic motion and transverse to the channel flow. The interaction between the moving block and the channel flow destroys and suppresses the velocity and thermal boundary layers on the heat surface periodically. Various ratios of the Richardson numbers ($Gr/Re^2$) are simulated. The results show that under a higher velocity of the channel flow and a lower magnitude of $Gr/Re^2$, the enhancement of heat transfer rate is better. Oppositely, under a lower velocity of the channel flow and a higher magnitude of $Gr/Re^2$, the effect of natural convection driven by the buoyancy force is stronger and it is unfavorable to the heat transfer. A counter effect of the heat transfer rate is observed. These phenomena which are seldom analyzed before by numerical simulation are carried out in this study.

**Keywords:** Mixed convection, Three-dimensional channel flow, Enhancement of heat transfer, Moving boundary.

## 1. INTRODUCTION

A problem of mixed convection of a heat surface in a vertical channel flow is usually of practical importance and is widely considered in the design of devices such as heat exchangers, nuclear reactors, and solar energy system. Thus an effective method for improving the heat transfer performance of mixed convection in the channel flow is indisputable.

Mixed convection can be divided to three types by directions of a buoyancy force and a channel flow. One is the cross flow which means the direction of the buoyancy force is vertical to the direction of the channel flow. Najam *et al*. [1] presented a numerical study of laminar unsteady mixed convection in a two dimensional horizontal channel containing heating blocks periodically mounted on its lower wall while its upper wall was maintained cold at a constant temperature. The effect of the forced flow on natural convection cells was studied for different values of the Reynolds number, Rayleigh number, and the relative height of the blocks. Kitamura *et al*. [2] conducted experimental investigations of combined convective flows of air induced around uniformly heated, horizontal cylinders. The results showed that separation points gradually shifted from those of forced convection to the top edge of the cylinder with increasing wall heat fluxes and overall Nusselt numbers as well as separation points could be predicted with a non-dimensional parameter.

The aiding flow is another type of mixed convection which signifies that the direction of the buoyancy force is the same as the channel flow. Gau *et al*. [3] investigated Buoyancy-assisted convection flow and heat transfer processes in a heated vertical channel experimentally. Reversed flows were visualized experimentally, as well the effects and phenomena of the bourancy parameter were also observed. Desrayaud *et al*. [4] researched laminar mixed convection in an entry region of symmetrically heated, vertical plate channels. Reversal flows were observed when the Richardson number was more than 1. The effects of various Reynolds numbers were also investigated and the reversal flow was unobvious as long as the increase of the Reynolds number.

The opposing flow is the other type of mixed convection which is defined as that direction of the buoyancy force is opposite to the direction of the channel flow. Martinez-Suastegui *et al*. [5] solved unsteady two-dimensional Navier–Stokes and energy equations for transient laminar mixed convection in an asymmetrically and differentially heated vertical channel of a finite length subject to an opposing buoyancy. Results illustrated the effects of the Richardson number and Reynolds number on the overall flow structure and the Nusselt number from the heated surface. Joye [6] investigated mixed convection heat transfer in a vertical tube with opposing flow experimentally. The data presented for the opposing flow with the Grashorf number as a parameter showed a reduced heat transfer

* Corresponding author (wsfu@mail.nctu.edu.tw)


DOI : 10.1017/jmech.2012.111

enhancement as the Grashorf number was lowered. A correlation of the Nusselt number and Reynolds number of results fitted the former articles quite well. To sum up, a three- dimensional model with the Boussinesq assumption is very few in the past articles.

About studies of heat transfer enhancement, in the past Bergles [7,8] had reviewed the development in convective heat transfer augmentation in detail. It is well-known methods of enlargement of heat dissipation surface [9-13], disturbance of flow field [14-19] and vibration of heat surface [20-23] are most usually applied to enhance heat transfer rate of the channel flow and the results of the above methods are remarkable and available. Due to the speedy formation of thermal boundary layer along the flow direction, the heat transfer rate of the above methods seems to only have a superior heat transfer rate in the upstream region. The increment of heat transfer in the downstream region is still low. Therefore, Fu *et al*. [24-25] presented a new method in which a block moved back and forth on a heat plate and destroyed the thermal boundary layer forming on the heat plate simultaneously to enhance the heat transfer rate of the heat plate, and heat transfer rates were promoted successfully. Then the method of using a block moving periodically on the heat surface is regarded as a worthwhile way.

Since natural convection induced by a temperature difference with a high magnitude of $Gr/Re^2$ is notable and the movement of the block causes the spaces distributed in both sides of the block to be contracted and enlarged simultaneously. The compressibility of fluid is then considered. For resolving the viscous compressible fluid in a low speed flow correctly, several related numerical methods had been proposed. Due to the difficulty of convergence and the limitation of CFL (Courant-Friedrichs-Levy) condition, the time step scale is too small to maintain the calculation in the explicit numerical method. Besides, the inefficiency of calculation caused by the stiff situation occurs easily in an implicit numerical method. For overcoming these defects mentioned above, Briley *et al*. [26] adopted the preconditioning method to improve the efficiency of calculation for a low Mach number flow, and the implicit numerical method was used to resolve the convergent problem of the Navier-Stokes equations. Turkel [27] developed and applied a preconditioning matrix into problems of compressible and incompressible flows. Choi and Merkel [28] investigated convergent problems induced by the stiff situation and factorization error when an implicit numerical method was used to solve an inviscid flow under a low Mach number flow. Furthermore, the convergent problem of the Mach number of 0.05 was successfully resolved by using the precondition matrix. Choi and Merkel [29] proposed the adaptable preconditioning matrix to solve convergent problems of a viscous flow under a low Mach number situation. Roe [30] developed an averaged variables method for a compressible flow to solve discontinuous phenomenon occurring at a cell interface. This method has been widely used in solving compressible flow recently. Weiss and Smith [31] extended the research of Choi, applied the Roe scheme mentioned above with the preconditioning method into the solution method of three dimensional Navier-Stokes equations, and added the dual time stepping to resolve transient states of a low Mach number flow. Besides, The movement of the moving block which moves back and forth on the heat surface is transverse to the flow direction. Then the three dimensional model with moving boundaries is considered. The immersed boundary method developed by Peskin [32] and edited by substituting the Arbitrary Largrangian-Eulerian method of finite element scheme [22] is adopted to deal with the moving block and to avoid wasting lots of memory.

Therefore, the aim of the study investigates enhancement of heat transfer of aiding flow mixed convection in a three dimensional vertical channel with a moving block numerically. The immersed boundary method is adopted to treat the block moving transversely on the heat surface. For simulating high temperature difference conditions, the compressibility of fluid is taken into consideration instead of the Boussinesq assumption. Related methods of the Roe scheme [30], preconditioning [29] and dual time stepping [31] are used for solving a low speed compressible flow in the channel.The results show that under a higher velocity of the channel flow and a lower magnitude of $Gr/Re^2$, the enhancement of heat transfer rate is better and the maximum enhancement is about 30%. Oppositely, under a lower velocity of the channel flow and a higher magnitude of $Gr/Re^2$, the effect of natural convection driven by the buoyancy force is stronger and it is unfavorable to the heat transfer. A counter effect of heat transfer rate is observed.

## 2. PHYSICAL MODEL

A physical model investigated in this study is a three-dimensional vertical channel and shown in Fig. 1. The length, width, and height of the channel are $w_2$, $w_1$, and $l_1$, respectively. A heat surface ABFE of which the width, length, and temperature are $w_1$, $l_2$, and $T_h$, respectively, is installed on the $x_1x_3$ plane. The distances from the inlet and outlet to the heat surface are $l_3$ and $l_4$, respectively. Cooling fluid flows into the channel, and the uniform velocity and temperature of the cooling fluid are $u_0$ and $T_0$, respectively. The thermal and flowing conditions of the cooling fluid at the outlet are fully developed. A moving slender block which has width $w_3$, length $l_2$, and height $h$ is set on the heat surface. In order to avoid the impediment of channel flow in the regions near both vertical walls, the slender block moves at the constant speed of $v_b$ from the point of $P_r$ to the point of $P_l$, and the distances from the right and left walls to the points of $P_r$ and $P_l$ are the same and equal to 1/4 $w_1$. The purpose of the moving slender block is to destroy the thermal boundary layer forming on the heat surface, and then the height of the moving block is higher than the thickness of the thermal boundary layer. Except the heat surface, the other surfaces including the moving slender block are

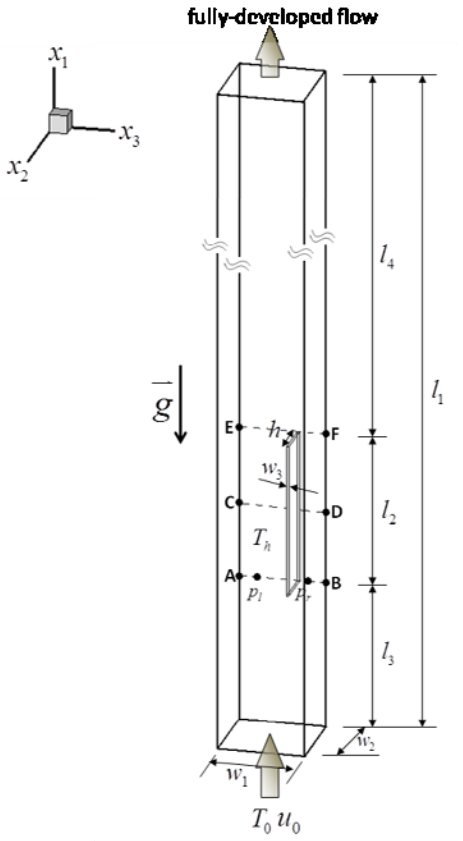


Fig. 1 Physical model

adiabatic. Laminar forced convection is studied exclusively in this work, and effects of a turbulence on the heat transfer mechanisms of the heat surface are neglected. According to Trong [33], the governing equations are expressed as follows.

$$\frac{\partial U}{\partial t}+\frac{\partial F}{\partial x}+\frac{\partial G}{\partial y}+\frac{\partial \mathrm{H}}{\partial z}=S \tag{1}$$

The quantities included in $U$, $F_i$ and $S$ are separately shown in the following equations.

$$U=\begin{pmatrix}\rho\\ \rho u_1\\ \rho u_2\\ \rho u_3\\ \rho e\end{pmatrix} \tag{2}$$

and

$$F_i=\begin{pmatrix}\rho u_i\\ \rho u_i\,u_1+P\delta_{i1}-\mu A_{i1}\\ \rho u_i\,u_2+P\delta_{i2}-\mu A_{i2}\\ \rho u_i\,u_3+P\delta_{i3}-\mu A_{i3}\\ (\rho e+P)\,u_i-\mu A_{ij}\,u_j-\lambda\dfrac{\partial T}{\partial x_i}\end{pmatrix},\quad \forall i=1,\ 2,\ 3 \tag{3}$$

$$S=\begin{pmatrix}0\\ 0\\ -(\rho-\rho_0)\,g\\ 0\\ -(\rho-\rho_0)\,gv\end{pmatrix} \tag{4}$$

where $A_{ij}=\dfrac{\partial u_j}{\partial x_i}+\dfrac{\partial u_j}{\partial x_i}$ and the ideal gas equation is written by

$$P=\rho RT \tag{5}$$

The Sutherland's law is adopted to evaluate the viscosity and the thermal conductivity as follows.

$$\mu(T)=\mu_0\left(\frac{T}{T_0}\right)^{\frac{2}{3}}\frac{T_0+110}{T+110} \tag{6}$$

$$k(T)=\frac{\mu(T)\,\gamma R}{(\gamma-1)\,\mathrm{Pr}}$$

where $\rho_0$ = 1.1842kg/m$^3$, $\mu_0 = 1.85 \times 10^{-5}$N·s/m$^2$, $T_0 = 298.0592K$, $\gamma = 1.4$, $R$ = 287J/kg/K and Pr = 0.72.

To simplify the analysis of results, the following dimensionless variables are made.

$$\begin{aligned}&X_1=\frac{x_1}{w_1},\ X_2=\frac{x_2}{w_1},\ X_3=\frac{x_3}{w_1},\\ &U_1=\frac{u_1}{u_0},\ U_2=\frac{u_2}{u_0},\ U_3=\frac{u_3}{u_0},\ V_b=\frac{v_b}{u_0}\end{aligned} \tag{7}$$

The compressibility and viscosity of the working fluid are considered, and the definition of the Reynolds number Re and the local Nusselt number $Nu_{x_3}$ on a certain cross section of the $x_2x_3$ plane of the heat surface is defined as follows.

$$\mathrm{Re}=\frac{\rho_0\,u_0\,w_1}{\mu_0} \tag{8a}$$

$$Nu_{X_3}=\frac{w_1}{k_0(T_h-T_0)}\left[k(T)\frac{\partial T}{\partial x_2}\right] \tag{8b}$$

Since the conditions of the channel flow are dynamic and unsteady throughout, in Eq. (8b) the temperature difference of $(T_h - T_f)$ which is usually used in a convection channel flow is conveniently substituted by $(T_h - T_0)$.

## 3. NUMERICAL METHOD

Accompanying with the usage of the Roe and preconditioning methods, two other effective methods are used together to avoid the occurrence of inefficiency and inaccuracy in computing processes. One is the method of three dimensional curvilinear coordinate ($\xi$, $\eta$, $\zeta$) to be used for clustering the grids near the heat

surface. The dual-time-stepping process is the other one to improve the efficiency of convergence. The original governing Eq. (1) is then transformed into the following equation.

$$\Gamma\frac{\partial U_p}{\partial\tau}+\frac{\partial U}{\partial t}+\frac{\partial F_1}{\partial\xi}+\frac{\partial F_2}{\partial\eta}+\frac{\partial F_3}{\partial\zeta}=S \tag{9}$$

where $\Gamma$ is the preconditioning matrix derived by Weiss *et al*. [31], and $U_p$ is the primitive form [$P$, $u_1$, $u_2$, $u_3$, $T$]/$J$ in which $J$ is the Jacobian matrix. $\tau$ and $t$ are an artificial and a physical times, respectively, $U$ is the conservative form of ($\rho$, $\rho u_1$, $\rho u_2$, $\rho u_3$, $\rho e$) / $J$.

To discretize Eqs. (9), (10) is obtained. Terms of $\partial U_p/\partial\tau$ and $\partial U/\partial t$ are differentiated by a first order forward difference and a second order backward difference, respectively, and terms of $\partial F_1/\partial\xi$, $\partial F_2/\partial\eta$, and $\partial F_3/\partial\zeta$ are differentiated by a central difference.

$$\begin{aligned}&\Gamma\frac{U_p^{k+1}-U_p^k}{\Delta\tau}+\frac{3U^{k+1}-4U^n+U^{n-1}}{2\Delta t}\\&+\frac{1}{\Delta\xi}(F_{1_{i+\frac{1}{2},j,k}}^{k+1}-F_{1_{i-\frac{1}{2},j,k}}^{k+1})+\frac{1}{\Delta\eta}(F_{2_{i,j+\frac{1}{2},k}}^{k+1}-F_{2_{i,j-\frac{1}{2},k}}^{k+1})\\&+\frac{1}{\Delta\zeta}(F_{3_{i,j,k+\frac{1}{2}}}^{k+1}-F_{3_{i,j,k-\frac{1}{2}}}^{k+1})=S^k\end{aligned} \tag{10}$$

In which superscripts of $k$ and $n$ indicate iteration numbers of the artificial time and a proceeding step of real time, respectively. When the term of the artificial time $\partial U_p/\partial\tau$ is convergent to $\varepsilon(=10^{-3})$, Eq. (10) is automatically transfered into the Navier-Stokes equations and the values at the iteration number of ($k$ + 1) of the artificial time in Eq. (10) substantially become the values at the proceeding step of ($n$ + 1) of the real time.

Afterward terms of $U^{k+1}$ and $F_i^{k+1}$ in Eq. (10) are necessary to be linearized and expressed as follows, respectively.

$$U^{k+1}=U^k+M\Delta U_p \tag{11}$$

where $M=\dfrac{\partial U}{\partial U_p}$ and $\Delta U_p=U_p^{k+1}-U_p^k$

$$F_1^{K+1}=F_1^K+A_p\,\Delta U_p \tag{12}$$

where $A_p=\partial F_1^k/\partial U_p$ is the flux Jacobian and the same methods for $B_p=\partial F_2^k/\partial U_p$ and $C_p=\partial F_3^k/\partial U_p$ are used in linearization of $F_2^{K+1}$ and $F_3^{K+1}$, respectively.

To substitute Eqs. (11) and (12) into Eq. (10), the following equation is obtained.

$$\begin{aligned}&\Gamma\frac{\Delta U_p}{\Delta\tau}+\frac{3(U^k+M\Delta U_p)-4U^n+U^{n-1}}{2\Delta t}\\&+\delta_\xi(F_1^k+A_p\,\Delta U_p)+\delta_\eta(F_2^k+B_p\,\Delta U_p)\\&+\delta_\zeta(F_3^k+C_p\,\Delta U_p)=S^k\end{aligned} \tag{13}$$

where $\delta_\xi$, $\delta_\eta$, and $\delta_\zeta$ are central-difference operators.

Equation (13) can be rearranged as the following form.

$$\left[\Gamma\frac{I}{\Delta\tau}+M\frac{3}{2\Delta t}+(\delta_\xi A_p+\delta_\eta B_p+\delta_\zeta C_p)\right]\Delta U_p=R^k \tag{14}$$

where $R^k=-\left(\dfrac{3U^k-4U^n+U^{n-1}}{2\Delta t}\right)-(\delta_\xi F_1^k+\delta_\eta F_2^k+\delta_\zeta F_3^k)+S^k$, $I$ is an unit matrix.

To divide the $\Gamma$ in both sides, the following equation is obtained.

$$\left[\frac{I}{\Delta\tau}+\Gamma^{-1}M\frac{3}{2\Delta t}+\Gamma^{-1}(\delta_\xi A_p^k+\delta_\eta B_p^k+\delta_\zeta C_p^k)\right]\Delta U_p=\Gamma^{-1}R^k \tag{15}$$

The solver of Eq. (16) is the LUSGS implicit method proposed by Yoon *et al*. [34] which is used to solve Eq. (15).

$$\begin{aligned}A_p&=\Gamma^{-1}A_p^k\\B_p&=\Gamma^{-1}B_p^k\\B_p&=\Gamma^{-1}C_p^k\end{aligned} \tag{16}$$

As for computation of $R^k=-(3U^k-4U^n+U^{n-1}/2\Delta t)-(\delta_\xi F_1^k+\delta_\eta F_2^k+\delta_\zeta F_3^k)+S^k$ in the RHS (right hand side) of Eq. (14), the terms of $F_i$ in Eq. (3) based on Cartesian coordinate can be divided into two parts. One is an inviscid term $F_{\text{inviscid}}$.

$$F_{\text{inviscid}}=\begin{pmatrix}\rho u_i\\ \rho u_i\,u_1+P\delta_{i1}\\ \rho u_i\,u_2+P\delta_{i2}\\ \rho u_i\,u_3+P\delta_{i3}\\ (\rho e+P)\,u_i\end{pmatrix} \tag{17}$$

The other is a viscous term $F_{\text{viscous}}$.

$$F_{\text{viscous}}=-\begin{pmatrix}0\\ \mu A_{i1}\\ \mu A_{i2}\\ \mu A_{i3}\\ \mu A_{ij}\,u_j+\lambda\dfrac{\partial T}{\partial x_i}\end{pmatrix} \tag{18}$$

The upwind difference scheme developed by Roe [30] is employed in discretization of the term of $F_{\text{inviscid}}$ at the cells interface ($i$ + 1/2) and expressed as follows at a low Mach number situation.

$$F_{\text{inviscid},i+\frac{1}{2}} = \frac{1}{2}(F_R + F_L) - \frac{1}{2}\varepsilon\left\{|\Gamma^{-1}A_p|\Delta U_P\right\} \tag{19}$$

In which ε is less than 0.1 and appropriate for a turbulent flow.

The high order MUSCL scheme proposed by Abalakin *et al*. [35] is used to compute the Eq. (19).

The derivative terms of $A_{ij} = \frac{\partial u_j}{\partial x_i} + \frac{\partial u_j}{\partial x_i}$ in Eq. (18) are computed by a fourth order central difference.

$$\frac{\partial u}{\partial x} = \frac{u_{i-2} - 8u_{i-1} + 8u_{i+1} - u_{i+2}}{12\Delta x} + o(\Delta x^4) \tag{20}$$

Advantages of usage of the LUSGS implicit method are to improve efficiency and decease artificial dissipation.

The object investigated in this study is to use the moving slender block to destroy the thermal boundary layer on the heat surface for succeeding in improvement of the heat transfer rate of the heat surface. Thus the object is belong to a kind of moving boundary problem and appropriately resolved by two methods. One is the arbitrary Lagrangian and Eulerian method, and the other is the immersed boundary method. A three-dimensional compressible flow is considered, and then the immersed boundary method based on a finite difference scheme is adopted. The immersed boundary concept method was originally presented in the pioneering work of Peskin [32]. More recently, the application and simplified versions of the method were presented in [36-38]. Instead of using complicated boundary fitted grids to define the moving motion, the immersed boundary method actually copes with the geometry of the solid body and the moving motion by means of suitably defined body force applied to the discrete set of the momentum equations. The Navier-Stokes equations with the force terms mentioned above introduced through the boundary conditions can be written as follows.

$$\frac{\partial U}{\partial t} = -\left(\frac{\partial F_1}{\partial x_1} + \frac{\partial F_2}{\partial x_2} + \frac{\partial F_3}{\partial x_3}\right) + \rho F_B \tag{21}$$

where $F_B$ is the body force term computed at every time step, so that the velocity distribution on an arbitrary surface is equal to the function of $V_s$.

$$U^{n+1} = U^n + \Delta t(Rhs + \rho F_B) = V_s \tag{22}$$

where *Rhs* includes all the pressure gradient, advection and diffusion terms. In case of a stationary solid body with a no-slip boundary condition, $V_s$ = 0 along the boundary. In this study, the specified velocity $V_s$ is equal to the velocity of the moving slender block. In order to lead the velocity of the next time step $U^{n+1}$ to be equal to the desired value $V_s$ on the immersed boundary, the source term $F_B$ of Eq. (21) can be expressed as follows.

$$F_B = \frac{1}{\rho}\left(\frac{V_s - U^n}{\Delta t} - Rhs\right) \tag{23}$$

This force term is direct in the sense that the desired value of the velocity is imposed directly on the boundary without any empiricism [38]. The main advantage of the immersed boundary method is that the force $F_B$ can be prescribed on a regular grid and the accuracy and efficiency of the solution procedure on simple rectilinear grids are maintained.

## 4. RESULTS AND DISCUSSION

According to numerical tests, the related length variables are determined and shown as follows.

$$\begin{aligned} &w_2 / w_1 = 1 \\ &w_3 / w_1 = 0.05 \\ &h / w_1 = 0.5 \\ &l_1 / w_1 = 15 \\ &l_2 / w_1 = l_3 / w_1 = 2.25 \\ &l_4 = 10.5 \end{aligned} \tag{24}$$

Due to the convenience of the computation of the immersed boundary, the computational time step is equal to the time of the block moves one grid in the $x_3$ direction which is changing with the changing of the Reynolds number and the velocity of the moving block.

In Fig. 2, the velocity distribution of this study at the outlet of the channel compared with the analytical solution [39] expressed in the following Eq. (25) is indicated.

$$u_1(x_2, x_3) = \frac{4w_1^2}{\mu\pi^3}\left(-\frac{dp}{dx_1}\right)\sum_{i=1,3,5,\ldots}^{\infty}(-1)^{\frac{(i-1)}{2}}\left[1 - \frac{\cosh\left(\frac{i\pi x_3}{w_1}\right)}{\cosh\left(\frac{i\pi}{2w_1}\right)}\right] \times \frac{\cos\left(\frac{i\pi x_2}{w_1}\right)}{i^3} \tag{25}$$

In the central region, a slight difference exists between both the results, and in the other regions both the results have good agreements.

Situations investigated in the study are tabulated in Tables 1 and 2. The temperature differences of the cases of Tables 1 and 2 are 12K and 100K, respectively. In addition, the Richardson numbers of both tables are 0.11, 1.3 and 11.5, respectively.

For cases of the aiding flow, it is well-know that the effect of the buoyancy force is more significant in the higher Richardson number. In Fig. 3(a), the temperature field of the middle cross section of the channel on the $x_1x_2$ plane shows the better heat transfer because stronger force convection brings the colder fluid through the whole channel in the case of the lower Richardson number ($Gr/\mathrm{Re}^2$ = 0.11). For the case of the higher Richardson number ($Gr/\mathrm{Re}^2$ = 11.5), the same cross section of the temperature field mentioned above is shown in Fig. 3(b). The effect of natural convection due to the stronger buoyancy force induces some impediments to the transmission of the colder fluid from the inlet.

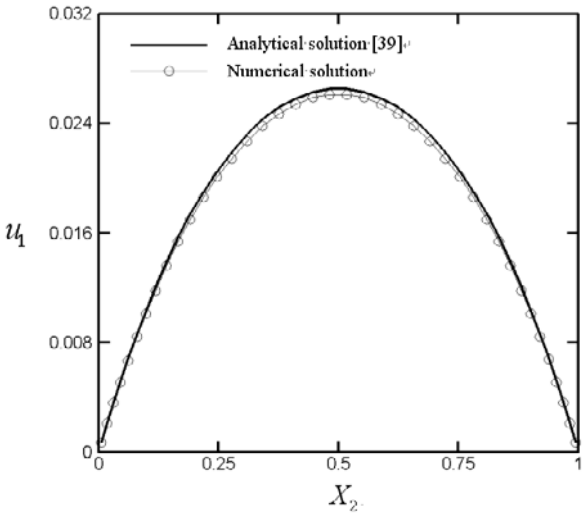


Fig. 2 Comparison of present results with analytical solution [39]

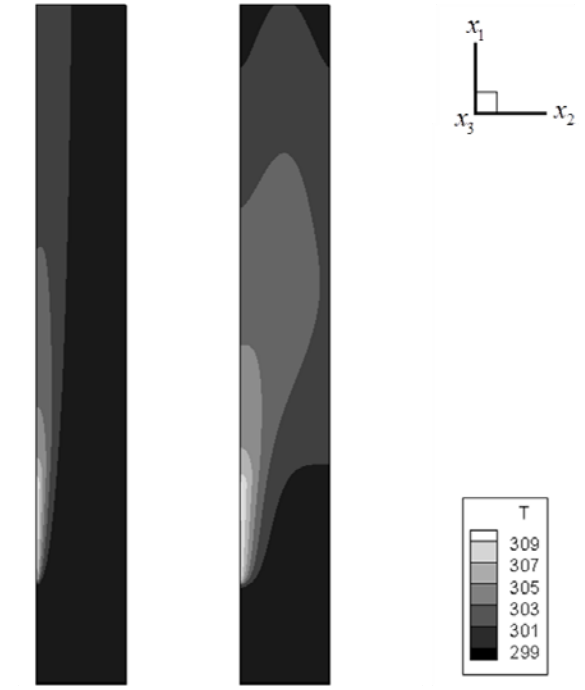


(a) $Gr/\mathrm{Re}^2 = 0.11$ (b) $Gr/\mathrm{Re}^2 = 11.5$

Fig. 3 The temperature field of the middle cross section of the channel

Table 1 Cases of temperature difference 12K ($\Delta T$ = 12K)

| Re | $Gr/\mathrm{Re}^2$ | Velocity of the block ($V_b$) |
|---|---|---|
| 350 | 0.11 | 1/4 |
| 350 | 0.11 | 1/2 |
| 100 | 1.3 | 1/4 |
| 100 | 1.3 | 1/2 |
| 35 | 11.5 | 1/4 |
| 35 | 11.5 | 1/2 |

Table 2 Cases of temperature difference 100K ($\Delta T$ = 100K)

| Re | $Gr/\mathrm{Re}^2$ | Velocity of the block ($V_b$) |
|---|---|---|
| 1000 | 0.11 | 1/4 |
| 1000 | 0.11 | 1/2 |
| 300 | 1.3 | 1/4 |
| 300 | 1.3 | 1/2 |
| 100 | 11.5 | 1/4 |
| 100 | 11.5 | 1/2 |

In Fig. 4, velocity fields on the $x_2x_3$ plane at the front (AB), middle (CD), and back (EF) cross sections under the situation of Re = 350, $Gr/\mathrm{Re}^2 = 0.11$ and $V_b = 1/2$ are indicated, respectively. In these figures, the slender block finishes a last periodic movement from $P_l$ to $P_r$ position and just starts to execute a next new periodic movement from $P_r$ to $P_l$ position. Shown in Fig. 4(a), the channel flow collides with the front edge of the slender block all the times, and velocities of fluids around the slender block are affected by mutual effects of the channel flow and the movement of the block. Velocity directions of fluids on the left side of the block are the same as that of the movement of the block. As for behaviors of fluids on the narrow right side of the block, some fluids supplement a vacant space caused by the movement of block and flow behind the block, and some other fluids are suppressed by the channel flow and flow upward.

Velocity fields on the middle (CD) and back (EF) cross sections are indicated in Figs. 4(b) and 4(c), respectively. Since both cross sections have certain distances away from the front edge of the heat surface, and for an instant the effect of the channel flow does not reach both the cross sections yet. As well, the effect of the last periodic motion of the block still leaves, and fluids near the left side of the block then flow to the right side. That fluids near the right side of the block supplement the vacant space caused by the movement of block is similar to that shown in Fig. 4(a). A circulation induced by the interaction of the streamwise channel flow and the movement of the block is observed, and the behavior of the circulation is like a rolling dish and moves with the block closely.

Shown in Fig. 5, the distributions of isothermal lines on the front, middle, and back cross sections which are separately corresponding to the cross sections indicated in Fig. 4 are indicated, respectively. In Fig. 5(a), on the front cross section the channel flow which is not heated yet touches the heat surface first, the distribution of isothermal lines is plainly dense close to the heat surface. The space of the right side of the block is much narrower than that of the left side of the block that causes the amount of streamwise channel flow to flow through the space of the left side of the block to be more than that to flow through the space of the right side of the block. Therefore, the distribution of isothermal lines of the right side of the block is a bit sparser than that of the left side of the block.

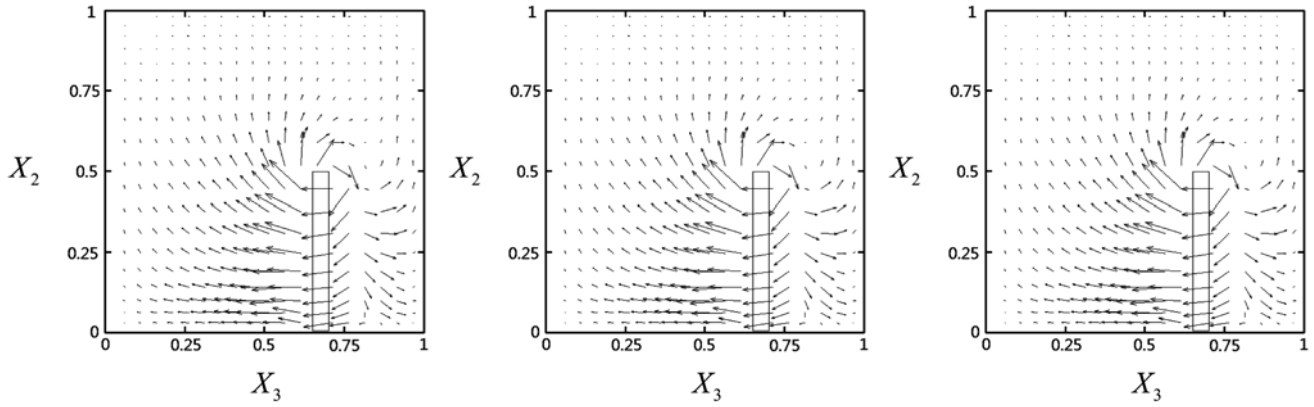


(a) The front cross section (AB) (b) The middle cross section (CD) (c) The rear cross section (EF)

Fig. 4 Distributions of velocity field ($Gr/\mathrm{Re}^2 = 0.11$, Re = 350)

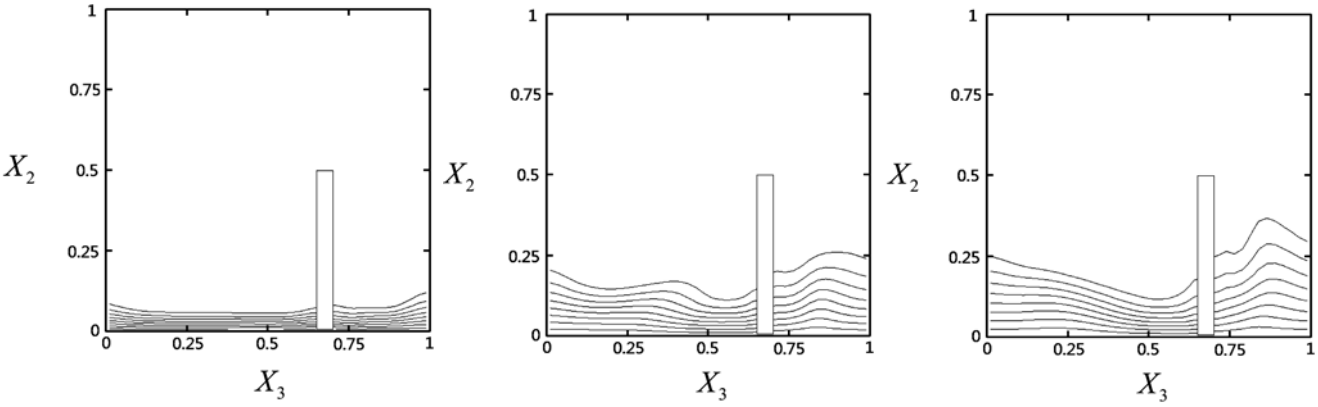


(a) The front cross section (AB) (b) The middle cross section (CD) (c) The rear cross section (EF)

Fig. 5 Distributions of temperature field ($Gr/\mathrm{Re}^2 = 0.11$)

In Figs. 5(b) and 5(c), both distributions of isothermal lines of middle and back cross sections which are in a downstream region are sparser than that of the front cross section. Besides, on both cross sections the distributions of isothermal lines of the right side of the block are sparser than those of the left side of the block, and the reason is the same as that mentioned above. The circulation induced by the interaction between the channel flow and block movement is somewhat like a rolling dish, then the distribution of isothermal lines is suppressed by this circulation and a concave is found on the left side of the block. This phenomenon is observed on both cross sections.

In Fig. 6, local Nusselt numbers $Nu_{X_3}$ distributed along heat surfaces of front, middle, and back cross sections are shown, respectively. Dashed lines indicate the situation without a moving block and solid lines indicate the situation with the moving block. Shown in Fig. 6(a), the channel flow first touches the heat surface at the front cross section and it is very advantageous to the heat transfer rate of the heat surface. Therefore, local Nusselt numbers of solid lines are larger than those of dashed lines in the left region of the block. In the right region of the block, this region is narrower and less fluids flow through the region that leads the heat transfer rate of the heat surface to get worse. Then in this region local Nusselt numbers of the solid lines are oppositely smaller than those of the dashed lines.

Both middle and back cross sections are gradually far away from the front edge of the heat surface, distributions of local Nusselt numbers indicated by the dashed lines on those two cross sections are naturally smaller than that of the front cross section. Due to the existence of the circulation in the left region near the block, thermal boundary layers of the heat surface are suppressed by the circulation that causes the distributions of local Nusselt numbers indicated by the solid lines relative to those indicated by the dashed lines to be enhanced and to become larger magnitude. In the region near the left wall of this cross section, Nusselt numbers of solid lines are slightly smaller than those of dashed lines due to the less amount of flow near the corner of the channel which are induced by the circulation. In the narrow right region of the block, the mobility of the fluid in this region is inferior and it is needless to say the distributions of local Nusselt numbers indicated by the solid lines are much smaller than those indicated by the dashed lines.

In Fig. 7, the block is moving to the center of the heat surface, velocity fields on the front, middle, and back cross sections are indicated, respectively. A large and remarkable circulation zone is observed in each

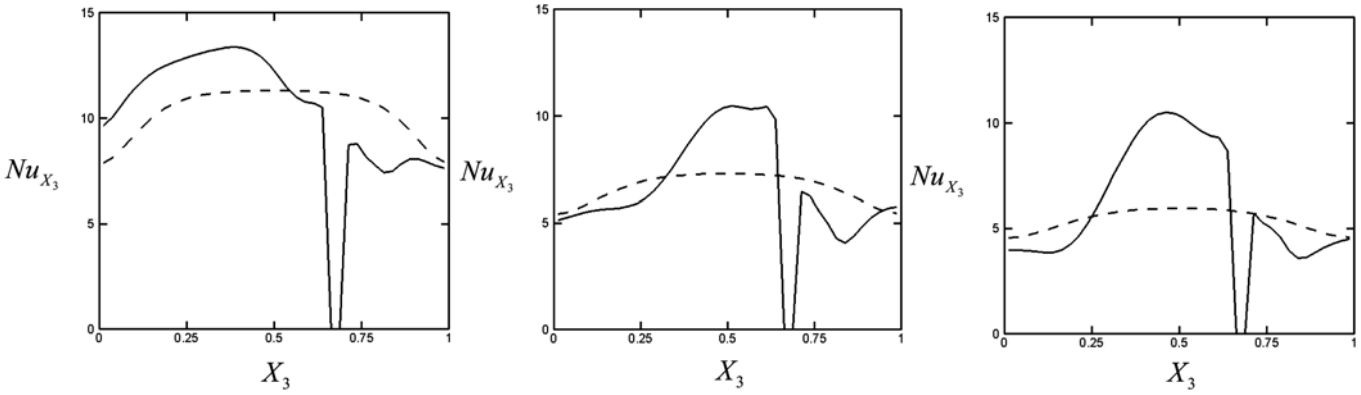


(a) The front cross section (AB) (b) The middle cross section (CD) (c) The rear cross section (EF)

Fig. 6 Distributions of local Nusselt numbers ($Gr/\mathrm{Re}^2 = 0.11$)

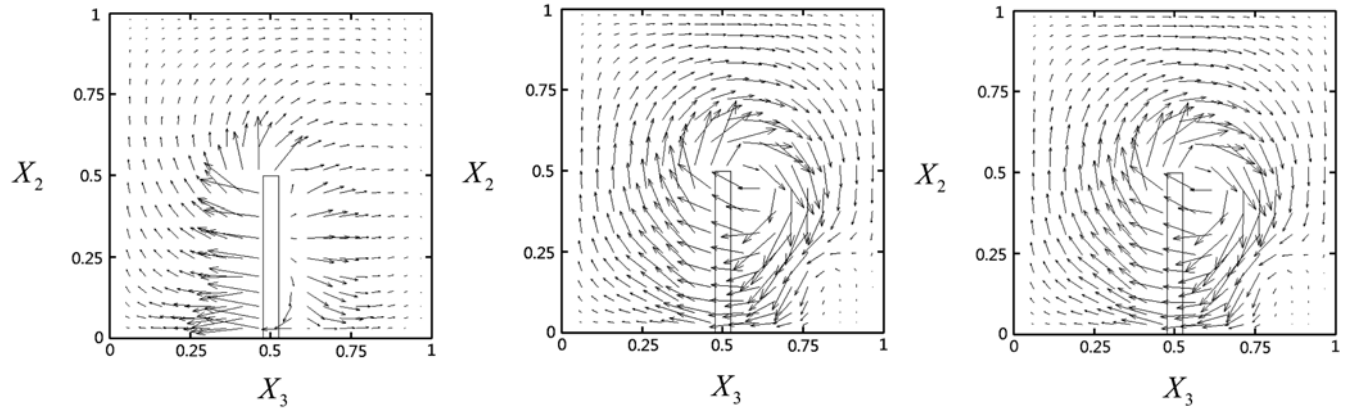


(a) The front cross section (AB) (b) The middle cross section (CD) (c) The rear cross section (EF)

Fig. 7 Distributions of velocity field ($Gr/\mathrm{Re}^2 = 0.11$)

cross section, and the block is included in it. In the right bottom region of the block, fluids affected by the circulation flow tightly along the bottom surface and closely behind the block. These behaviors are advantageous to the heat transfer rate of the heat surface. Near the left bottom region of the block fluids are pushed forward by the moving block, and the fluids still flow tightly along the heat surface except the middle cross section. Due to the interaction of the channel flow and the block, the fluids in the middle cross section have a slight trend to flow upward.

Shown in Fig. 8, the distributions of isothermal lines on the front, middle, and back cross sections are indicated, respectively. According to descriptions of velocity fields mentioned above, the isothermal lines which have a small distance away the block are denser than those in other regions. Therefore, concaves on distributions of isothermal lines indicated in Figs. 5(b) and 5(c) are also observed.

In Fig. 9, the distributions of local Nusselt numbers on the front, middle, and back cross sections are shown, respectively. Based on the distributions of the isothermal lines mentioned above, in each cross section the distribution of local Nusselt numbers of the right region of block is much larger than that of the results without a moving block. In Fig. 9(b), Nusselt numbers indicated by solid lines are smaller than those indicated by dashed lines due to the behaviors of flow fields mentioned in Fig. 7.

The following figures show the results of Re = 35, $Gr/\mathrm{Re}^2 = 11.5$ and $V_b = 1/2$. The velocity fields shown in Fig. 10 are similar to those shown in Fig. 4. Due to both lower velocities of the channel flow and moving block, the interaction of both velocities becomes weaker that directly causes distributions of isothermal lines of cross sections shown in Fig. 11 to be sparser than those shown in Fig. 5 although the velocity fields are similar. Therefore, based on the reasons mentioned above distributions of local Nusselt numbers indicated in Fig. 12 are then much different from those indicated in Fig. 6. Relative to the case without a moving block indicated by dashed lines, the heat transfer rates shown in Fig. 12 are worse on each cross section even in the left region of the block.

Shown in Fig. 13, the block moves to the center of the cross section. The similar circulation zone mentioned in Fig. 7 is also observed in each cross section. Then the variations of the distributions of the isothermal lines shown in Fig. 14 are much sparser than those shown in Fig. 8. This phenomenon decreases the heat transfer rates of both the left and right regions of the block apparently. Shown in Fig. 15, no matter in the left or the right region Nusselt numbers indicated by solid lines are lower than those indicated by dashed lines. These phenomena are due to the stronger buoyancy effect in this case of a higher $Gr/\mathrm{Re}^2$.

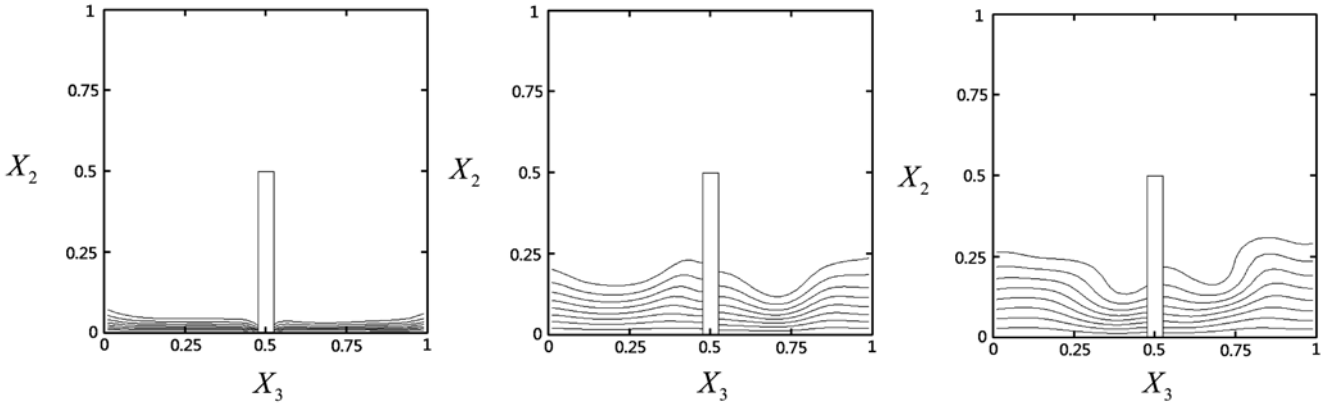


(a) The front cross section (AB) (b) The middle cross section (CD) (c) The rear cross section (EF)

Fig. 8 Distributions of temperature field ($Gr$/Re$^2$ = 0.11)

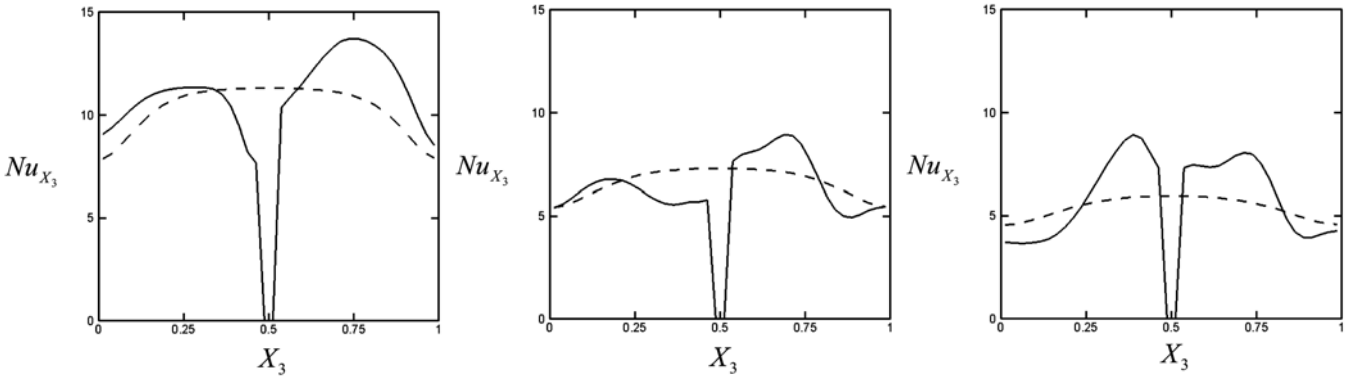


(a) The front cross section (AB) (b) The middle cross section (CD) (c) The rear cross section (EF)

Fig. 9 Distributions of local Nusselt numbers ($Gr$/Re$^2$ = 0.11)

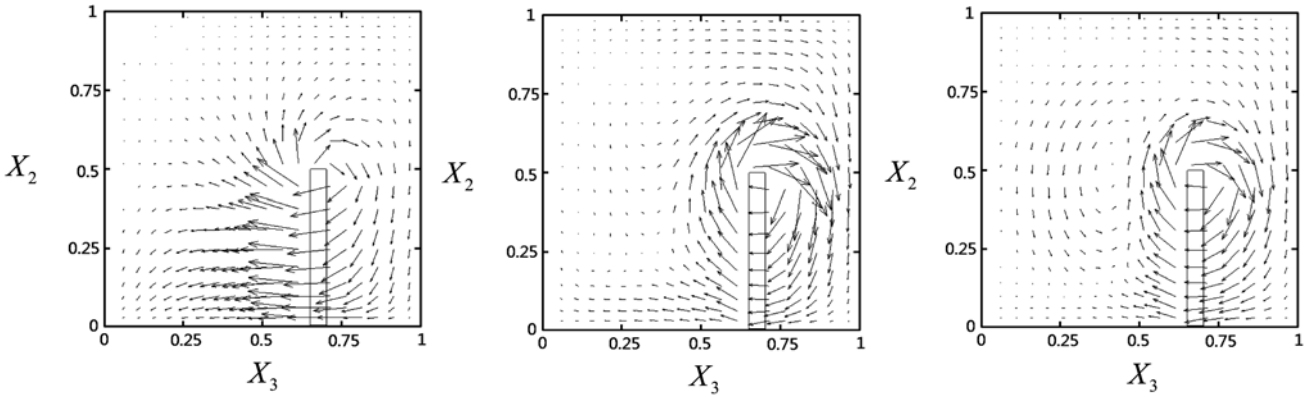


(a) The front cross section (AB) (b) The middle cross section (CD) (c) The rear cross section (EF)

Fig. 10 Distributions of velocity field ($Gr$/Re$^2$ = 11.5)

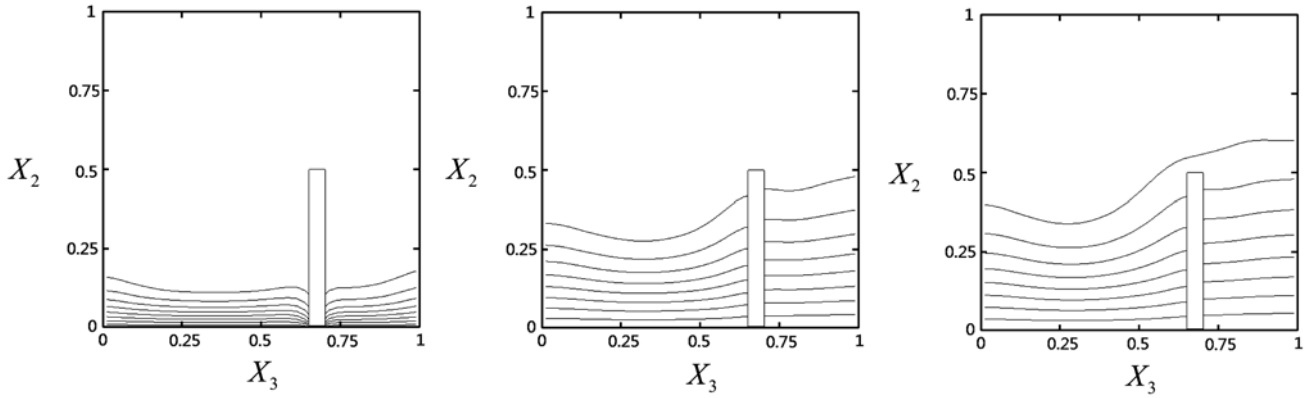


(a) The front cross section (AB) (b) The middle cross section (CD) (c) The rear cross section (EF)

Fig. 11 Distributions of temperature field ($Gr$/Re$^2$ = 11.5)

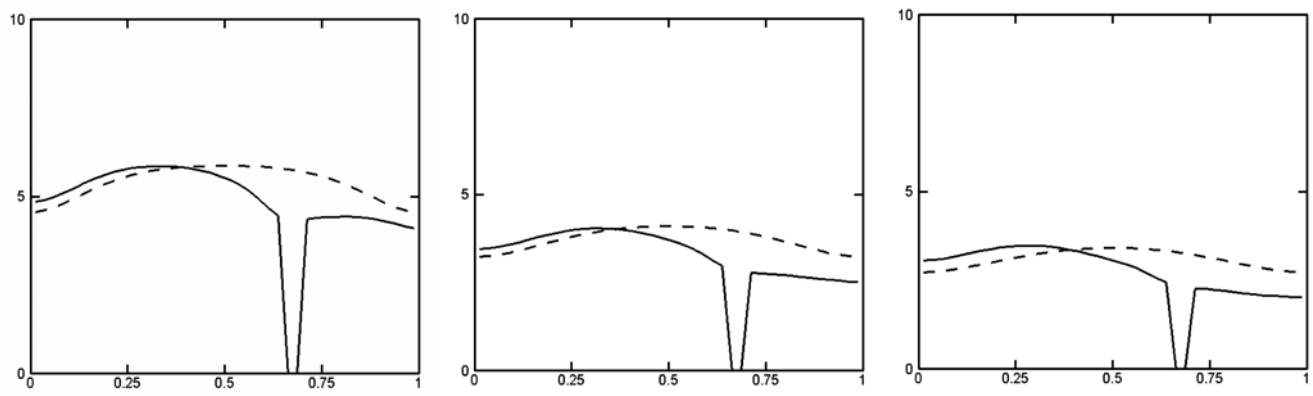

(a) The front cross section (AB) (b) The middle cross section (CD) (c) The rear cross section (EF)

Fig. 12 Distributions of local Nusselt numbers ($Gr/\mathrm{Re}^2 = 11.5$)

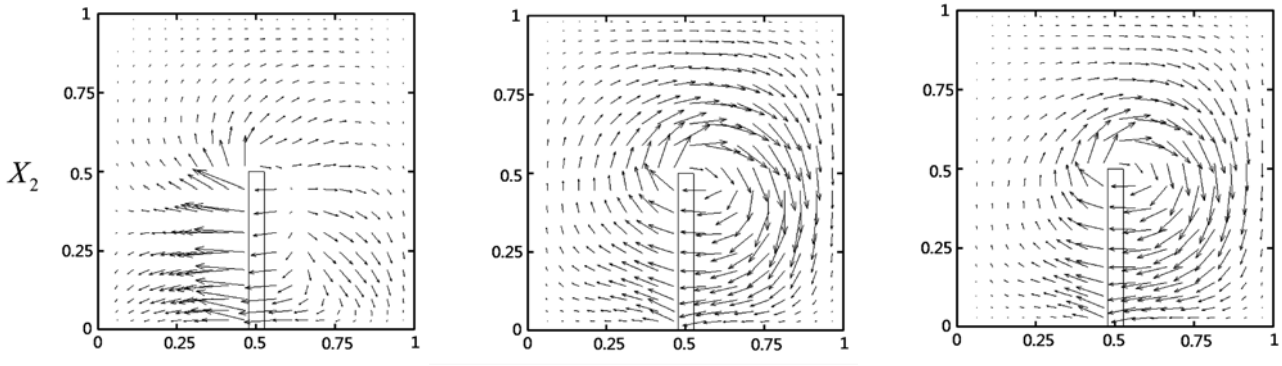


(a) The front cross section (AB) (b) The middle cross section (CD) (c) The rear cross section (EF)

Fig. 13 Distributions of velocity field ($Gr/\mathrm{Re}^2 = 11.5$)

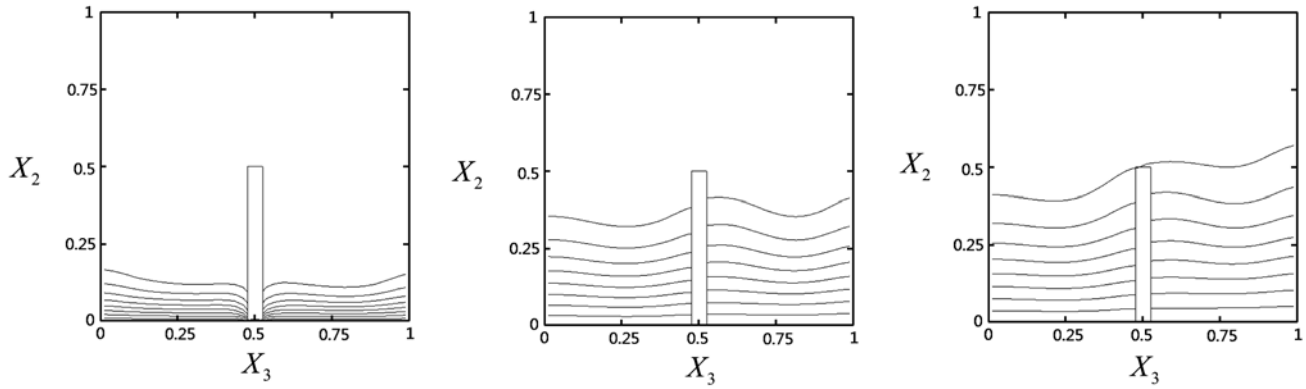


(a) The front cross section (AB) (b) The middle cross section (CD) (c) The rear cross section (EF)

Fig. 14 Distributions of temperature field ($Gr/\mathrm{Re}^2 = 11.5$)

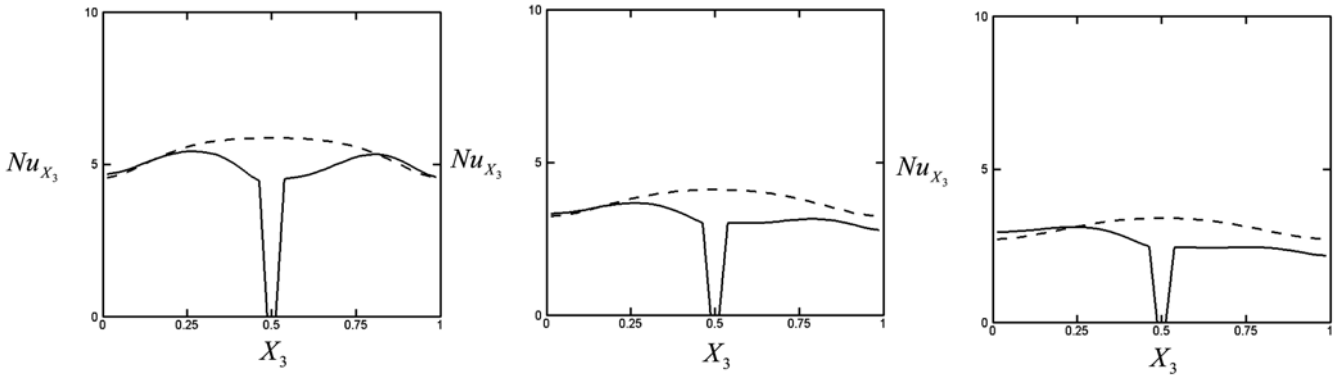


(a) The front cross section (AB) (b) The middle cross section (CD) (c) The rear cross section (EF)

Fig. 15 Distributions of local Nusselt numbers ($Gr/\mathrm{Re}^2 = 11.5$)

Natural convection induced by the heat surface drive the flow near the heat bottom surface upward and the channel flow cannot touch the heat surface directly.

In Figs. 16 (a) and 16(b), comparisons of the average local Nusselt numbers of the heat surface along the streamwise direction at $Gr/\mathrm{Re}^2$ = 0.11 and 11.5 situations are indicated, respectively. The definition of the average local Nusselt number of $\overline{Nu}_{x_1}$ is expressed as follows.

$$\overline{Nu}_{x_1} = \frac{1}{t_p}\int_t Nu_{x_1}\,dt\ ,\quad t_p = \text{time of a cycle} \tag{26}$$

Relative to the results shown in Fig. 16(b), in Fig. 16(a) the velocity of the channel flow is quicker which causes the effect of the interaction between the channel flow and the moving block to become strong. As a result, the enhancement of the heat transfer rate is achieved in the whole region. In Fig. 16(b), due to the slow velocities of the channel flow and natural convection induced by a stronger buoyancy force, the upward flow near the bottom surface impedes the channel flow to touch the heat surface. Then the enhancement of the heat transfer rate is difficult to achieve on the whole heat surface.

Enhancement of an average heat transfer rate of a cycle En tabulated in Tables 3 and 4 are calculated by the following equation.

$$En = \frac{(Nu)_{\text{with block}} - (Nu)_{\text{without block}}}{(Nu)_{\text{without block}}} \tag{27}$$

where $(Nu) = \dfrac{1}{t_p}\displaystyle\int_t \overline{Nu}\ dt$ , $t_p$ = time of a cycle

Enhancements shown in Table 3 are the cases with a higher temperature difference of 100K. The interaction of the channel flow and the moving block is stronger under the low $Gr/\mathrm{Re}^2$ situation, the strong interaction directly causes the heat transfer rate to increase and remarkable enhancements of the heat transfer rate are achieved about 30% in one of them. Oppositely, under a lower temperature difference of 12K shown in Table 4, the interaction is worse due to the weaker forced convection and it is disadvantageous to the heat transfer. The best enhancement of heat transfer in this situation is only about 10%, and most of enhancements of this table are negative.

Table 3 Enhancement of heat transfer rate of a cycle *En* ($\Delta T$ = 100K)

| Re | $Gr/\mathrm{Re}^2$ | $V_b$ | $\overline{Nu}$ | *En* |
|---|---|---|---|---|
| 1000 | 0.11 | N/A | 13.16 | N/A |
| 1000 | 0.11 | 1/4 | 14.38 | 9.3% |
| 1000 | 0.11 | 1/2 | 17.32 | 31.6% |
| 300 | 1.3 | N/A | 8.70 | N/A |
| 300 | 1.3 | 1/4 | 8.82 | 1.4% |
| 300 | 1.3 | 1/2 | 9.13 | 5.0% |
| 100 | 11.5 | N/A | 7.35 | N/A |
| 100 | 11.5 | 1/4 | 7.11 | –3.2% |
| 100 | 11.5 | 1/2 | 7.22 | –1.7% |

Table 4 Enhancement of heat transfer rate of a cycle *En* ($\Delta T$ = 12K)

| Re | $Gr/\mathrm{Re}^2$ | $V_b$ | $\overline{Nu}$ | *En* |
|---|---|---|---|---|
| 350 | 0.11 | N/A | 8.02 | N/A |
| 350 | 0.11 | 1/4 | 8.40 | 4.9% |
| 350 | 0.11 | 1/2 | 8.82 | 10.0% |
| 100 | 1.3 | N/A | 5.40 | N/A |
| 100 | 1.3 | 1/4 | 5.18 | –4.0% |
| 100 | 1.3 | 1/2 | 5.26 | –2.6% |
| 35 | 11.5 | N/A | 4.38 | N/A |
| 35 | 11.5 | 1/4 | 3.95 | –9.7% |
| 35 | 11.5 | 1/2 | 4.03 | –8% |

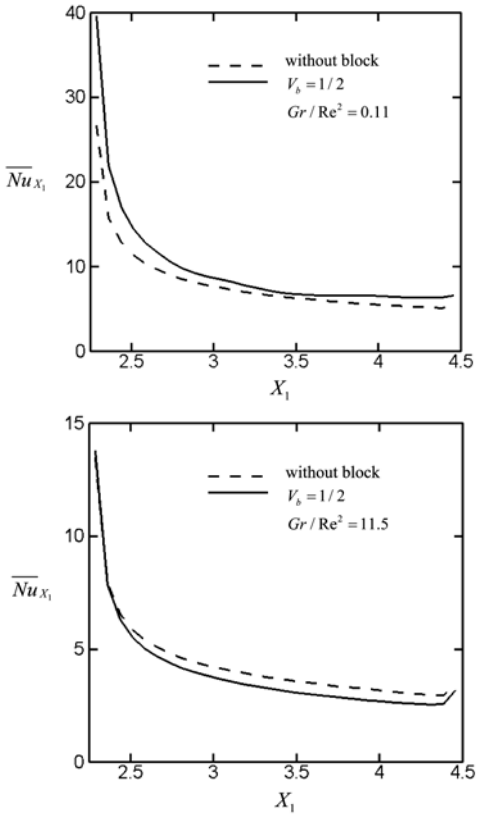


Fig. 16 Comparisons of the average local Nusselt numbers of heat surface along the centerline of streamwise direction

## 5. CONCLUSIONS

Enhancement of heat transfer of a vertical channel flow with insertion of a moving block is investigated. Several conclusions are summarized as follows.

1. Usage of a moving block to enhance a heat transfer rate of a channel flow is remarkable especially in the downstream region of the channel flow.
2. A case of a lower Richardson number has a better enhancement of heat transfer due to the stronger interaction between the moving block and the channel flow.
3. A counter-effect is observed in a case of a higher Richardson number because the stronger buoyancy force impedes the slow channel flow to touch the heat surface.

## ACKNOWLEDGEMENTS

The authors gratefully acknowledge the support of the Natural Science Council, Taiwan, ROC under Contact NSC-99-2221-E-009-058


## NOMENCLATURES

*En* enhancement of the average heat transfer rate of the heat surface of a cycle defined in Eq. (27)

$g$ acceleration of gravity (m/s$^2$)
$Gr$ Grashof number
$h$ dimensional height of the slender block (m)
$k$ thermal conductivity (W/m·K)
$l_1$ dimensional length of the channel (m)
$l_2$ dimensional length of the slender block (m)
$l_3$ the distance between the inlet and the heat surface (m)
$l_4$ the distance between the outlet and the heat surface (m)
$M$ local Mach number
$Nu_{X_3}$ Nusselt number defined in Eq. (8b)
$\overline{Nu}_{X_1}$ average Nusselt number defined in Eq. (26)
$(Nu)$ average Nusselt number defined in Eq. (27)
$R$ gas constant (J/kg·K)
Re Reynolds number definfed in Eq. (8a)
$t$ time ($s$)
$T$ temperature (K)
$T_0$ temperature of surroundings (K)
$T_f$ film temperature (K)
$T_h$ temperature of heat surface (K)
$u_1, u_2, u_3$ velocities in $x_1$, $x_2$ and $x_3$ directions (m/s)
$U_1, U_2, U_3$ dimensionless velocities in $X_1$, $X_2$ and $X_3$ directions
$v_b$ moving velocity of the slender block (m/s)
$V_b$ dimensionless velocity of the slender block
$w_1$ dimensional width of the channel (m)
$w_2$ dimensional height of the channel (m)
$w_3$ dimensional width of the slender block (m)
$x, y, z$ Cartesian coordinates (m)
$X_1, X_2, X_3$ dimensionless Cartesian coordinates

### Greek symbol

$\gamma$ specific heat ratio
$\xi, \eta, \zeta$ curvilinear coordinates
$\theta$ dimensionless temperature
$\mu$ viscosity ($N \cdot s/m^2$)
$\mu_0$ Surrounding viscosity ($N \cdot s/m^2$)
$\rho$ density (kg/m$^3$)
$\rho_0$ surrounding density (kg/m$^3$)

## REFERENCES


1. Najam, M., Amahmid, A., Hasnaoui, M. and Alami, M. El., "Unsteady Mixed Convection in a Horizontal Channel with Rectangular Blocks Periodically Distributed on its Lower Wall," *International Journal of Heat and Fluid Flow*, **24**, pp. 726–735 (2003).
2. Kitamura, K., Mototani, K. and Kimura, F., "Heat Transfer of Combined Forced and Natural Convection from Horizontal Cylinder to Air," *Heat Transfer*, **36**, pp. 474–488 (2007).
3. Gau, C. Yih, K. A. and Aung, W., "Reversed Flow Structure and Heat Transfer Measurements for Bouyancy Assisted Convection in a Heated Vertical Duct," *Journal of Heat Transfer*, ASME, **114**, No. 4, pp. 928–935 (1992).
4. Desrayaud, G. and Lauriat, G., "Flow Reversal of Laminar Mixed Convection in the Entry Region of Symmetrically Heated, Vertical Plate Channels," *International Journal of Thermal Sciences*, **48**, pp. 2036–2045 (2009).
5. Martinez-Suastegui, L. and Trevino, C., "Transient Laminar Opposing Mixed Convection in a Differentially and Asymmetrically Heated Vertical Channel of Finite Length," *International Journal of Heat and Mass Transfer*, **51**, pp. 5991–6005 (2008).
6. Joye, D. D., "Comparison of Correlations and Experiment in Opposing Flow, Mixed Convection Heat Transfer in a Vertical Tube with Grashorf Number Variation," *International Journal of Heat and Mass Transfer*, **39**, pp. 1033–1038 (1996).
7. Bergles, A. E., "Recent Development in Convective Heat Transfer Augmentation," *Applied. Mechanics Reviews*, **26**, pp. 675–682 (1973).
8. Bergles, A. E., "Survey and Evaluation of Techniques to Augment Convective Heat and MassTrandfer," *Heat Mass Transfer*, **1**, pp. 331–424 (1969).
9. Chen, X. and Sutton, W. H., "Enhancement of heat transfer: Combined Convection and Radiation in the Entrance Region of Circular Ducts with Porous Inserts," *International Journal of Heat and Mass Transfer*, **48**, pp. 5460–5474 (2005).
10. Yucel, N. and Guven, R. T., "Forced-convection Cooling Enhancement of Heated Elements in a Parallel-plate Channels Using Porous Inserts," *Numerical Heat Transfer A*, **51**, pp. 293–312(2007).
11. Gharebaghi, M. and Sezai, I., "Enhancement of Heat Transfer in Latent Heat Storage Modules with Internal Fins," *Numerical Heat Transfer A*, **53**, pp. 749–765 (2008).
12. Zeng, Y. and Vafai, K., "An Investigation of Convective Cooling of an Array of Channel-mounted Obstacles," *Numerical Heat Transfer A*, **55**, pp. 967–982 (2009).
13. Parthasarathy, P., Talukdar, P. and Kishore, V. R., "Enhancement of Heat Transfer with Porous/solid Insert for Laminar Flow of a Participating Gas in a 3-D

Square Duct," *Numerical Heat Transfer A*, **56**, pp. 764–784 (2009).
14. Zhang, J. and Dalton, C., "Interaction of a Steady Approach Flow and a Circular Cylinder Undergoing Forced Ascillation," *Journal of Fluids Engineering*, **119**, pp. 808–813 (1997).
15. Zhu, C., Liang, H., Sun, D., Wang, L. and Zhang, Y., "Numerical Study of Interactions of Vortices Generated by Vortex Generators and Their Effects on Heat Transfer Enhancement," *Numerical Heat Transfer A*, **50**, pp. 345–360 (2006).
16. Jayavel, S. and Tiwari, S., "Numerical Study of Flow and Heat Transfer for Flow Past Inline Circular Tubes Built in a Rectangular Channel in the Presence of Vortex Generators," *Numerical Heat Transfer A*, **54**, pp. 777–797 (2008).
17. Chen, Y. Y., Song, K. W., Wang, L. B. and Sun, D. L., "Comparisons of Local Experimental Results of Heat Transfer Enhancement of a Flat Tube Bank Fun with Vortex Generators," *Numerical Heat Transfer A*, **55**, pp. 144–162 (2009).
18. Huang, T. M., Gau, C. and Aung, W., "Flow and Mixed Convection Heat Transfer in a Divergent Heated Vertical Channel," *Journal of Heat Transfer*, ASME, **118**, pp. 605–615 (1996).
19. Su, J. H., Gau, C. and Yang, C. S., "Enhancement of Heat Transfer over a Cylinder by Acoustic Excitation," *AIAA, Journal of Thermophysics and Heat Transfer*, **20**, pp. 256–266 (2006).
20. Gau, C., Wu, J. M. and Liang, C. Y., "Heat Transfer Enhancement and Vortex Flow Structure over a Heated Cylinder Oscillating in Crossflow Direction," *Journal of Heat Transfer*, ASME, **121**, pp.789–795 (1999).
21. Gau, C., Wu, S. X. and Su, H. S., "Synchronization of Vortex Shedding and Heat Transfer Enhancement over a Heated Cylinder Oscillating with Small Amplitude in Streamwise Direction," *Journal of Heat Transfer*, ASME, **123**, pp. 1139–1148 (2001).
22. Fu, W. S. and Tong, B. H., "Numerical Investigation of Heat Transfer Characteristics of the Heated Blocks in the Channel with a Transversely Oscillating Cylinder," *International Journal of Heat and Mass Transfer*, **47**, pp. 341–351 (2004).
23. Li, J., "Numerical Approximation of Unsteady Natural Convection from a Vertical Flat Plate with a Surface Temperature Oscillation," *Numerical Heat Transfer A*, **46**, pp. 383–399 (2004).
24. Fu, W. S. and Wang, K. N., "An Investigation of a Block Moving Back and Forth on a Heat Plate under a Slot Jet," *International Journal of Heat and Mass Transfer*, **44**, pp. 2621–2631 (2001).
25. Fu, W. S., Tseng, C. C., Wang, K. N. and Huang, C. P., "An Experimental Investigation of a Block Moving Back and Forth on a Heat plate under a Slot Jet," *International Journal of Heat and Mass Transfer*, **50**, pp. 3224–3233 (2007).
26. Briley, W. R., McDonald, H. and Shamroth, S. J., "At Low Mach Number Euler Formulation and Application to Time Iterative LBI Schemes," *AIAA*, **21**, pp. 1467–1469 (1983).
27. Turkel, E., "Preconditioned Methods for Solving the Incompressible and Low Speed Compressible Equations," *Journal of Computational Physics*, **72**, pp. 277–298 (1987).
28. Choi, D. and Merkel, C. L., "Application of Time-iterative Schemes to Incompressible Flow," *AIAA,* **25**, pp. 1518–1524 (1985).
29. Choi, D. and Merkel, C. L., "The Application of Preconditioning in Viscous Flows," *Journal of Computational Physics*, **105**, pp. 207–223 (1993).
30. Roe, P. L., "Approximation Riemann Solver, Parameter Vectors, and Difference Schemes," *Journal of Computational Physics*, **43**, pp. 357–372 (1981).
31. Weiss, J. M. and Smith, W. A., "Preconditioning Applied to Variable and Constants Density Flows," *AIAA*, **33**, pp. 2050–2056 (1995).
32. Peskin, C. S., "Flow Patterns Around Heart Valves: A Numerical Method," *Journal of Computational Physics*, **10**, pp. 252–271 (1972).
33. Trong, T. B., "A Parallel Finite-Volume Algorithm for Large-Eddy Simulation of Turbulence Flows," *Computers and Fluids*, **29**, pp. 877–915 (2000).
34. Yoon, S. and Jameson, S., "Lower-upper Symmetric-Gauss-Seidel Method for the Euler and Navier-Stokes Equations," *AIAA*, **26**, pp. 1025–1026 (1988).
35. Abalakin, I., Dervieux, A. and Kozubskaya, T., "A Vertex Centered High Order MUSCL Scheme Applying to Linearized Euler Acoustics," *INRIA*, No4459 (2002).
36. Verzicco, R., Mohd-Yusof, J., Orlandi, P. and Haworth, D., "Les in Complex Geometries Using Boundary Body Forces," *AIAA*, **38**, pp. 427–433 (2000).
37. Grigoriadis, D. G. E., Bartzis, J. G. and Goulas, A., "LES of the Flow Past a Rectangular Cylinder Using a Immersed Boundary Concept," *International Journal for Numerical Methods in Fluids*, **41**, pp. 615–632 (2003).
38. Li, C. W. and Wang, L. L., "An Immersed Boundary Finite Difference Method for LES of Flow Around Bluff Shapes," *International Journal for Numerical Methods in Fluids*, **46**, pp. 85–107 (2004).
39. White, F. M., *Viscous Fluid Flow*, McGrawHill Co., Ltd., p. 113 (2006).

(Manuscript received December 9, 2011,
accepted for publication May 22, 2012.)